Absolute total one- and two-electron-transfer cross sections of O^{3+} and O^{2+} with CO at kilo-electron-volt energies

H. Gao, Z. Fang, and Victor H. S. Kwong
Department of Physics, University of Nevada, Las Vegas, 4505 Maryland Parkway, Las Vegas, Nevada 89154
(Received 21 August 2000; published 6 February 2001)

Absolute total one- and two-electron-transfer cross sections for O^{q+} $(q=3,2)$ with CO were measured at $\sim 1.5q$ keV energies. The measurement was carried out by a technique that combines a laser ablation ion source and a reflection time-of-flight mass spectrometer. The single- and double-electron capture cross sections for O^{3+} with CO are $(1.26\pm 0.18)\times 10^{-15}$ and $(0.72\pm 0.11)\times 10^{-15}$ cm^2, respectively. The single-electron capture cross section for O^{2+} with CO is $(0.76\pm 0.11)\times 10^{-15}$ cm^2.

DOI: 10.1103/PhysRevA.63.032704 PACS number(s): 34.70.+e, 32.80.Pj, 52.50.Jm, 95.30.Dr

I. INTRODUCTION

Charge-transfer processes between singly and multiply charged ions and neutral atoms and molecules are of considerable importance in astrophysics and fusion plasmas. Charge-transfer collisions between these ions and CO molecules are of particular interest because CO molecules have been found in a wide range of astrophysical objects and regions [1–4], and their presence can play an important role in the chemistry that controls the photon emission of that region. Measurements using CO as a target gas have been reported at eV energies with ions such as O^{2+}, He^+, and N^{2+} [5–8]. However, very few measurements have been made at keV energies (with H^+ and He^{2+}) [9]. The lack of data at this energy range limits our ability to determine the chemical processes in astrophysical plasmas and planetary objects. As a case in point, recent reports on the observations by the Rontgen x-ray satellite (ROSAT) and the Rossi x-ray Timing Explorer of extreme ultraviolet and x-ray emissions from the comet C/Hyakutake 1996 B2 have generated intense interest in the mechanisms of the x-ray source. Among these mechanisms, charge transfer between the minor/heavy solar wind ions such as O^{q+}, C^{q+}, and Si^{q+} and molecules such as CO and H_2O from the comet appears to be the most promising mechanism [10] to explain the source of soft x-ray emission. However, modeling such as that used by Haberli *et al.* [11] requires detailed and accurate single- and multielectron charge-transfer cross sections between minor/heavy solar wind ions and major cometary neutrals such as H_2O and CO. The lack of experimental and theoretical cross section data can compromise the accuracy of the model. In the case of Haberli *et al.* [11], the charge-transfer cross sections for O^{q+} and CO were assumed to be within 20% to 30% of the measured cross sections for O^{q+} and H_2. Although a reasonable agreement was found between the observed emissions and the results of the emission model, it is essential that these cross sections be measured accurately for further refinement of the model. The limited bandwidth of the ROSAT does not have enough resolution to identify all the emission lines. However, with NASA's Chanda x-ray observatory, its high-resolution capability enables us to resolve individual spectral lines, thus giving us a better insight into the emission line spectrum of future comets and the source of the emission line. These emission lines can be used to reveal the chemistry of comet atmospheres and solar wind. The correct interpretation of the emission lines is critically determined by the accuracy of the charge-exchange cross sections.

A facility that combines a laser ablation ion source and a reflection time-of-flight mass spectrometer (RTOFMS) has demonstrated its suitability in measuring charge-transfer cross sections at keV energies [12]. This paper will focus on absolute total cross section measurements for the following charge-transfer processes at $\sim 1.5q$ keV energies:

$$O^{3+} + CO \rightarrow O^{2+} + \text{products (ion or ion+neutral)}, \quad (1)$$

$$O^{3+} + CO \rightarrow O^{+} + \text{products (ion or ion+neutral)}, \quad (2)$$

$$O^{2+} + CO \rightarrow O^{+} + \text{products (ion or ion+neutral)}, \quad (3)$$

where reactions (1) and (3) are single-electron capture (SC) processes and reaction (2) is a double-electron capture (DC) process.

II. EXPERIMENTAL METHOD

Figure 1 shows the schematic of a reflection time-of-flight mass spectrometer with a laser ablation ion source. A detailed description of the experimental facility can be found in Ref. [12]. Oxygen ions were produced by laser ablation of a high-purity (97%) solid Ta_2O_5 target mounted on a rotatable manipulator inside the vacuum chamber. The energy of the 50 ns Nd:YAG (yttrium aluminum garnet) laser pulse was 40 mJ. The laser beam was focused on the ablation target with an $f=33$ cm lens at an incident angle of 45°. At this power density, O^{q+} ions with $q\leqslant 5$ were routinely produced. The laser ablation target and the front grid of the RTOFMS were grounded (see Fig. 1). The ions of the laser ablation plasmas were extracted into the incident drift tube through a small aperture of the extractor which marks the entrance to the RTOFMS. The extractor and the incident drift tube were both biased at $V_0=-1500$ V relative to the ground. Since ions of charge q acquire additional kinetic energy $\delta E=-qeV_0$ from the extraction field, ions of different q will have different drift velocities in the field-free incident drift tube, and will be separated in their time of flight according to their mass-to-charge ratio. However, ions produced by laser

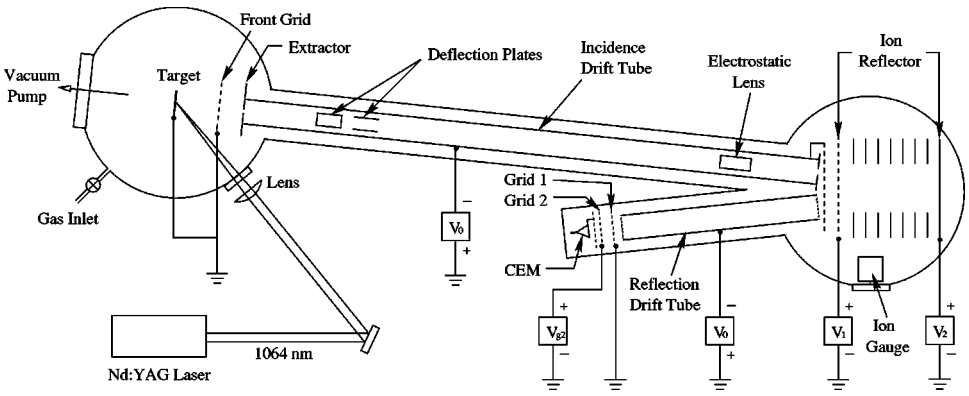

FIG. 1. The schematic of the reflection time-of-flight mass spectrometer (RTOFMS).

ablation have a wide range of initial kinetic energies. This spread of initial kinetic energy can limit the mass resolution of the ions. To improve the mass resolution further refinement on the TOF mass spectrometer is required. This refinement was accomplished by reflecting the ions 168° into a reflection drift tube at the end of the incident drift tube. The reflector assembly consists of a highly transparent front plate and a solid back plate. Between them there are several evenly spaced potential-gradient ring electrodes to maintain a uniform electric field across the reflector assembly. With this setup, ions with higher initial kinetic energy penetrate further into the reflector assembly before they are reflected into the reflection drift tube. The extra path taken by the more energetic ions allows the slower ions to catch up in time. By choosing the appropriate potentials on the electrodes of the incident drift tube, the reflector assembly, and the reflection drift tube, ions of the same m/q but with different initial kinetic energies can arrive at the detector plane at about the same time [12].

The potentials of the front plate and the back plate of the reflector assembly were set at $V_1 = +10$ V and $V_2 = +600$ V, respectively. The reflection drift tube was floated at the same potential V_0 as the incident drift tube. The potentials applied to those electrodes were chosen for the optimum beam intensity and mass resolution of the reflected parent oxygen ions. Any product ions produced due to charge transfer between the oxygen ions and molecules inside the incident drift tube could not be reflected into the reflection drift tube because of the change in their charge states. The parent oxygen ions and only their product ions that were produced in the reflection drift tube as the result of the charge-exchange reaction were detected by a channel electron multiplier (CEM) detector located at the end of the reflection drift tube.

The parent O^{q+} ions can be identified by their TOF spectrum with $t \propto q^{-1/2}$. Figure 2 shows a mass spectrum of laser-produced oxygen ions in the RTOFMS. However, this TOF spectrum cannot be used to identify the ions such as $O^{(q-1)+}$ and $O^{(q-2)+}$ produced through single-electron capture and double-electron capture from their parent ion O^{q+}, since the energy transfer between O^{q+} and CO is negligibly small in the charge-transfer process. Product ions keep very similar kinetic energy $E_i - qeV_0$ (where E_i is the initial kinetic energy of the parent ion O^{q+} as produced by laser ablation) to their parent ions after the reaction inside the reflection drift tube. To distinguish the product ions from the parent ions, a retardation field was applied to the ions between the end of the reflection tube and the CEM detector (see Fig. 1). The ions were first retarded by the grounded grid 1. Because of their charge differences, the kinetic energies of the parent ions and the product ions, after passing through grid 1, were reduced to E_i, $E_i - eV_0$, and $E_i - 2eV_0$, for O^{q+}, $O^{(q-1)+}$, and $O^{(q-2)+}$, respectively. By applying an appropriate potential V_{g2} at grid 2, selected oxygen ions are allowed to reach the CEM. For example, if $qeV_{g2} > E_i$ and $(q-1)eV_{g2} < E_i - eV_0$, O^{q+} are blocked, and $O^{(q-1)+}$ and $O^{(q-2)+}$ can pass through grid 2 and thus be detected by the CEM. A similar argument can be used to determine the value of V_{g2} to further block $O^{(q-1)+}$ and $O^{(q-2)+}$. Depending on the reflector's setting, only ions that have initial kinetic energy E_i within a certain range can be reflected into the reflection drift tube. The reflecting trajectories of the ions in the ion reflector were analyzed to estimate E_i in this range. For O^{3+} ions the range of E_i is between 120 eV and 600 eV, and for O^{2+} ions it is between 80 eV and 400 eV. The values of V_{g2} were determined based on these E_i values and V_0.

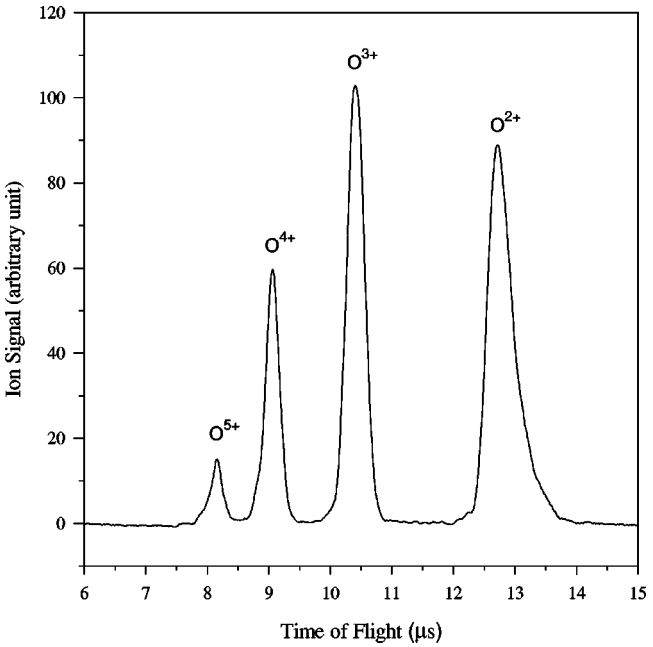

FIG. 2. Mass spectrum of the laser-produced oxygen ions in the RTOFMS.

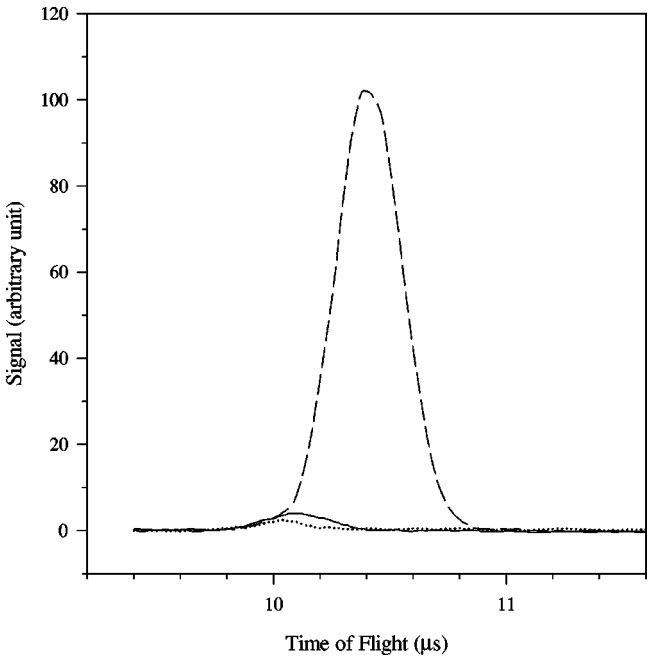

FIG. 3. Typical time-of-flight mass spectra in the measurement of the single-electron capture of O^{3+} with CO. Signals from large to small: laser-produced parent O^{3+} ion; products including O^{2+}, O^+, and O; and the products excluding O^{2+}.

During the $O^{3+}+CO$ measurement, by setting $V_{g2}=0$ V, all the parent ions and their product ions can pass through grid 2 and can be detected by the CEM. By setting $V_{g2}=+620$ V, parent O^{3+} ions were blocked while all the product ions and neutrals were allowed to pass. By setting $V_{g2}=+1100$ V, both the parent O^{3+} ions and the single-electron capture product ions O^{2+} were blocked while double-electron capture product ions and neutral O atoms formed by three-electron capture were allowed to pass. By setting $V_{g2}=+3700$ V, only neutral O could be detected. During $O^{2+}+CO$ measurement, $V_{g2}=+1100$ V was used to block parent O^{2+} ions, and $V_{g2}=+3700$ V was used to block the parent ions and the single-electron capture product ion O^+.

To reduce the systematic uncertainty on the ion signal due to the laser energy fluctuation and the changes in the target surface conditions, the measurements were carried out in cycles. In each cycle, V_{g2} was sequentially switched according to the calculated values set in the above discussion, i.e., 0 V, +620 V, and +1100 V for measurement of single-electron capture for O^{3+}; 0 V, +1100 V, and +3700 V for measurement of double-electron capture for O^{3+} and single-electron capture for O^{2+}. A total of about 3000 cycles was measured for each of these charge-transfer processes. The signals were recorded by a Tektronix digital oscilloscope, binned according to the switching sequence, and stored in a computer for later analysis. The typical superposition of the TOF spectra in the measurement of the single-electron capture of O^{3+} is shown in Fig. 3. Three distinct peaks are observed. The dominant peak represented by a dashed line corresponds to the parent ion O^{3+}, while the much weaker peak represented by a solid line corresponds to the product ions and the neutrals (O^{2+}, O^+, and O). The smallest peak, represented by a dotted line, corresponds to the product ions and the neutrals (O^+, and O). The differences in the signal intensities give the relative population of the parent ions and their product ions. A slight shifting of the TOF spectra toward shorter arrival time by the product ions is due to the higher average kinetic energies of the product ions in the retardation region.

The CO gas was admitted through a leak valve into the laser ablation vacuum chamber. The pressure of CO was measured by a calibrated ion gauge mounted at the reflection drift tube. The calibration method was discussed in a previous publication [13]. The CO pressure during the experiment was 2.0×10^{-5} Torr. The residual gas pressure (H_2, H_2O, and CO) of the reaction chamber was less than 2.0×10^{-9} Torr.

III. RESULTS AND DISCUSSION

A. Results

The electron capture cross section σ can be derived from the expressions

$$\frac{I_p}{I_0}=1-e^{-\sigma nL} \tag{4}$$

$$\text{and}\quad \sigma\approx\frac{I_p}{I_0 nL}, \tag{5}$$

where I_p is the signal intensity of the product oxygen ions, I_0 is the intensity of the parent O^{q+} ions, L is the interaction length of the reflection drift tube, and n is the density of the target CO gas. In Eq. (5), the approximation is valid because $I_p/I_0\ll1$ in our measurement, which also ensures single-collision conditions. The ion energies, according to E_i-qeV_0, are 4860 ± 240 eV for O^{3+} and 3240 ± 160 eV for O^{2+}. The measured charge-transfer cross sections are tabulated in Table I. Results of previous measurements with H_2 [14] are also listed for comparison.

B. CEM efficiency calibration

The gain efficiency of the detector depends on the ion charge state and its incident kinetic energy [14]. Since the CEM was operated in the analog mode, the gain efficiencies for O^{q+} ($q=1$, 2, 3) need to be determined experimentally. The calibration of the gain efficiency was carried out by measuring the pulse height distribution of an individual oxygen ion of a specific charge state and kinetic energy. This can be done by defocusing the ion beam with the electrostatic lens inside the incident drift tube until the individual ion can be detected. No significant difference in the efficiency has been observed.

C. Experimental uncertainty

The uncertainty of the gas pressure is estimated to be about 8% from the absolute ion gauge calibration, the uncertainty from the linearity of the channel electron multiplier and the preamplifier is about 2%, the uncertainty of pulse

TABLE I. Measured charge-transfer cross section σ for O^{q+} $(q=3,2)$ with CO and H_2.

Reaction	σ (cm^2)	Energy (eV/amu)	Reference	Method
$O^{2+}+CO$ (SC)	$(0.76\pm0.11)\times10^{-15}$	203 ± 10	This work	Experimental, RTOFMS and laser ion source
$O^{3+}+CO$ (SC)	$(1.26\pm0.18)\times10^{-15}$	304 ± 15		
$O^{3+}+CO$ (DC)	$(0.72\pm0.11)\times10^{-15}$	304 ± 15		
$O^{2+}+H_2$ (SC)	$(1.2\pm0.6)\times10^{-16}$	188	[14]	Experiment, ORNL-PIG source
$O^{3+}+H_2$ (SC)	$(9.4\pm1.5)\times10^{-16}$	281		

height calibration is about 10%, and the statistical uncertainty of the measured cross sections is about 6% for single-electron capture and 8% for double-electron capture. The total absolute uncertainty of the cross section is estimated to be about 14% for single-electron capture and 15% for double-electron capture after a quadrature sum.

D. Discussion of the results

It is well known that the existence of metastable states of the parent ion beam can, in some cases, dramatically change the measured electron capture cross sections [12,16]. The radiative lifetime of the metastable states of O^{2+} and O^{3+} ions ranges from 1.22 ms [17] to seconds [18], much longer than the flight time of the ion in the RTOFMS. This short transit time does not allow the ions to relax to their ground states prior to their reaction with CO. Such an unknown mixture of metastable and ground state ion species in the ion beam can lead to measured cross sections difficult to interpret. The metastable fractions in the pulsed laser plasma ion source have been investigated experimentally by Kwong and Fang [19] and Fang and Kwong [6,20] in their charge-transfer study of O^{2+} ($2s^2 2p^2\,{}^1D$ metastable state, $\tau\sim37$ s [18], $2s^2 2p^2\,{}^1S$ metastable state, $\tau\sim0.55$ s [18], and $2s^2 2p^2\,{}^3P$ ground state) using an ion trap, and Wang and Kwong [12] in their electron capture study of C^{2+} ($2s2p\,{}^3P_{0,1,2}$ metastable states, $\tau\geqslant8.26$ ms [21] and $2s^2\,{}^1S$ ground state) using the same facility for the current measurement. In both cases, their results are in agreement with the ground state measurements reported in [18,22]. This would suggest that the metastable fraction in the pulsed laser plasma ion souce is negligibly small. We conclude that there is no significant contribution by the metastable state ions in the present measurements.

Since neither theoretical nor experimental cross sections are available for comparison, the result will be compared with previously measured charge-transfer cross section for O^{q+} $(2\leqslant q\leqslant6)$ with H_2 at keV energies. The single-electron capture cross section for both O^{3+} and O^{2+} with H_2 is significantly smaller than the current measurement with CO as the target gas. This is not surprising. These cross sections are determined by the crossings of potential surfaces formed by an ion and a molecule during their brief collision; the CO molecule has a much more complex internal energy structure than has the hydrogen molecule, so it is quite conceivable that the number of crossings of the charge-transfer channels is higher for CO than for H_2, resulting in a higher probability for charge transfer to occur with CO. In the past, a number of quantal calculations on charge transfer between an atomic ion and a neutral atom have been made. However, very few charge transfer calculations between an atomic ion and a molecule have been reported [15]. One of the major difficulties in these calculations is the lack of accurate knowledge of these potential surfaces formed by the ion and molecule during their nonbinding collisions. Since the quasimolecule does not form permanently, the accuracy of the potential curves (surfaces) cannot be verified experimentally. Accurate cross sections are essential in the modeling of a wide range of fusion and astrophysical plasmas in which charge transfer take place.

In the computational modeling of x-ray emissions from comets [11], the measured electron capture cross sections between O^{q+} and H_2 [14] were used to calculate the cascading from high to low charge states. However, measurements of O^{3+} and O^{2+} with CO have shown that both single-electron capture cross sections are much larger than their reactions with H_2 by a factor of 1.34 and 6.33, respectively. Furthermore, the double-electron capture cross section is more than half of that for single-electron capture. The assumption that the cross sections for the reactions of higher charge states of oxygen ions with CO are within 20% to 30% of those with H_2 should be viewed with caution.

ACKNOWLEDGMENTS

The authors thank Bill O'Donnell and Jenniffer Pursley for their valuable technical assistance. This work was supported by the Nevada state EPSCoR program and by NASA under Grant No. NAG5-6727 to UNLV.

[1] J. Spyromilio, W. P. S. Meikle, R. C. M. Learner, and D. A. Allen, Nature (London) **334**, 327 (1988).

[2] P. J. McGregor, A. R. Hyland, and D. J. Hillier, Astrophys. J. **324**, 1071 (1988).

[3] J. S. Young, F. P. Schloerb, J. D. Kenney, and S. D. Lord, Astrophys. J. **304**, 443 (1986).

[4] D. E. Osterbrock, *Astrophysics of Gaseous Nebulae* (Freeman, New York, 1974), p. 211.

[5] Z. Fang and V. H. S. Kwong, Phys. Rev. A **55**, 440 (1997).
[6] Z. Fang and V. H. S. Kwong, Phys. Rev. A **51**, 1321 (1995).
[7] V. H. S. Kwong, D. Chen, and Z. Fang, Astrophys. J. **536**, 954 (2000).
[8] V. G. Anicich, J. B. Laudenslager, W. T. Huntress, Jr., and J. H. Futrell, J. Chem. Phys. **67**, 4340 (1977).
[9] M. B. Shah and H. B. Gilbody, J. Phys. B **23**, 1491 (1990).
[10] T. E. Cravens, Geophys. Res. Lett. **24**, 105 (1997).
[11] R. M. Haberli, T. I. Gombosi, D. L. De Zeeuw, M. R. Combi, and K. G. Powell, Science **276**, 939 (1997).
[12] J. Wang and V. H. S. Kwong, Rev. Sci. Instrum. **68**, 3712 (1997).
[13] V. H. S. Kwong *et al.*, Rev. Sci. Instrum. **61**, 1931 (1990).
[14] R. A. Phaneuf, I. Alvarez, F. W. Meyer, and D. H. Crandall, Phys. Rev. A **26**, 1892 (1982).
[15] P. C. Stancil, B. Zygelman, and K. Kurby, in *Proceedings of International Conference on the Physics of Electronic and Atomic Collisions, Vienna, Austria, 1997*, edited by F. Aumayr and H. Winter (World Scientific, Singapore, 1998), p. 537.
[16] T. K. McLaughlin, S. M. Wilson, R. W. McCullough, and H. B. Gilbody, J. Phys. B **23**, 737 (1990).
[17] B. C. Johnson, P. L. Smith, and R. D. Knight, Astrophys. J. **281**, 477 (1984).
[18] D. A. Church and H. M. Holzscheiter, Phys. Rev. A **40**, 54 (1989).
[19] V. H. S. Kwong and Z. Fang, Phys. Rev. Lett. **71**, 4127 (1993).
[20] Z. Fang and V. H. S. Kwong, Rev. Sci. Instrum. **65**, 2143 (1994).
[21] V. H. S. Kwong, Z. Fang, T. T. Gibbons, W. H. Parkinson, and P. L. Smith, Astrophys. J. **411**, 431 (1993).
[22] E. Unterreiter, J. Schweinzer, and H. Winter, J. Phys. B **24**, 1003 (1991).